Mapping the Linearly Polarized Spectral Line Emission around the Evolved Star IRC+10216

J.M. Girart[1]

N. Patel[2]

W. Vlemmings[3]

Ramprasad Rao[4]

ABSTRACT

We present spectro-polarimetric observations of several molecular lines obtained with the Submillimeter Array (SMA)[1] toward the carbon rich AGB star IRC+10216. We have detected and mapped the linear polarization of the CO 3–2, SiS 19–18 and CS 7–6 lines. The polarization arises at a distance of $\simeq$ 450 AU from the star and is blueshifted with respect the Stokes *I*. The SiS 19–18 polarization pattern appears to be consistent with a locally radial magnetic field configuration. However, the CO 3–2 and CS 7–6 line polarization suggests an overall complex magnetic field morphology within the envelope. This work demonstrates the feasibility of using spectro-polarimetric observations to carry out tomographic imaging of the magnetic field in circumstellar envelopes.

Subject headings: stars: AGB and post-AGB; stars: individual (IRC+10216, CW Leo); circumstellar matter; polarization; submillimeter: stars

1. Introduction

High mass loss during the AGB phase is one of the main contributors to the return of nucleo-synthesized material into the interstellar medium. A proper understanding of AGB mass loss is thus crucial for the study of the chemical evolution of the Galaxy. However, the exact mechanism or mechanisms responsible for the AGB mass loss is still not clear. After the AGB phase, the star evolves towards the Planetary Nebula (PN) phase. During this transition, fast winds are launched that interact with the earlier circumstellar envelope (CSE) that was created during the AGB. A large fraction of PNe are observed to be aspherical, and the origin of the asphericity is attributed to the influence of a binary companion, a disk, a magnetic field, or a

[1]Institut de Ciències de l'Espai, (CSIC-IEEC), Campus UAB, Facultat de Ciències, C5p 2, 08193 Bellaterra, Catalunya, Spain; girart@ice.cat

[2]Harvard-Smithsonian Center for Astrophysics, 60 Garden Street, Cambridge, MA 02138, USA

[3]Department of Earth and Space Sciences, Chalmers University of Technology, Onsala Space Observatory, SE-439 92 Onsala, Sweden

[4]Submillimeter Array, Academia Sinica Institute of Astronomy and Astrophysics, 645 N. Aohoku Place, Hilo, HI 96720, USA

[1]The SMA is a joint project between the Smithsonian Astrophysical Observatory and the Academia Sinica Institute of Astronomy and Astrophysics, and is funded by the Smithsonian Institution and the Academia Sinica.

combination of these. The exact onset of asphericity is still unknown, and high angular resolution molecular line observations indicate that several CSEs of AGB stars already display various degrees of asymmetry. The mechanism responsible for the creation of asymmetries is likely closely linked with that driving the mass loss and can be directly probed by high angular resolution observations of CSEs. In particular molecular line polarization observations are a unique tool to study potential asymmetries in the CSE and/or determine the shape of the circumstellar magnetic field.

The critical role of magnetic fields in star formation has been probed with direct observations of polarized dust continuum emission toward both low and high-mass star-forming regions (Girart et al. 2006, 2009; Rao et al. 2009). Similar techniques are difficult to apply for AGB stars due to the need for extremely high angular resolution ($< 0.''5$) and high sensitivity. A large number of studies have already been made of the magnetic field induced polarization of maser lines. These studies have revealed magnetic fields are present throughout the entire envelope. The SiO, H_2O and OH maser observations indicate that magnetic fields appear well ordered and the Zeeman splitting indicates the field strengths range from several Gauss close to the stellar surface to several mG at a few thousand AU (e.g., Etoka & Diamond 2004; Vlemmings et al. 2005, 2011; Herpin et al. 2006; Kemball et al. 2009; Amiri et al. 2011). However, masers probe only a limited number of lines of sight through the CSE and in most cases it is thus impossible to fully reconstruct the magnetic field morphology throughout the envelope. Furthermore, the most abundant masers are predominantly found around oxygen-right (M-type) limiting the available source sample. Non-masing molecular lines are however also predicted to be linearly polarized (e.g. Goldreich, & Kylafis 1981, 1982; Morris et al. 1985) to the level of a few percent, and can provide more extensive probes of the entire envelope.

Polarized emission has however conclusively been detected from for example CO in a number of star forming regions (e.g., Girart et al. 1999; Lai et al. 2003; Cortes et al. 2005; Forbrich et al. 2008). The molecular line polarization is due to the anisotropic radiation field from the central star imparting angular momentum on the molecules or from anisotropic level populations in the molecular magnetic substates when coupled with a magnetic field. Without a (non-radial) magnetic field, and assuming a spherically symmetric stellar wind, linear polarization should be radial or tangential and should only be detectable at lines of sight away from the central star (Morris et al. 1985). Thus, when these criteria are not met, molecular line polarization provides a unique diagnostic of magnetic field morphology and potential non-radial asymmetries in the stellar radiation field. Very recently, Vlemmings et al. (2012) have reported the detection of CO polarized emission toward IK Tau.

IRC+10216 (CW Leo) is a well studied AGB star with a high mass-loss rate, 3×10^{-5} $M_\odot$ yr^{-1}, and a terminal velocity of 15 km s^{-1} (e.g. Young et al. 1993). Due to the relatively close distance of 150 pc (Crosas & Menten 1997), this star provides an ideal laboratory for studies of circumstellar chemistry (Tenenbaum et al. 2010; Patel et al. 2011). Unlike typical Mira variables, there are no masers associated with this source, except perhaps a transition of SiS which may be a weak maser (Fonfría Expósito et al. 2006). The dusty envelope of IRC+10216 shows arc-like structures in scattered light (Mauron & Huggins 1999) which extend over more than $1'$ in angular radius. Closer to the star, dust emission shows asymmetrical structures over scales of $2''$ (Men'shchikov et al. 2001; Menut et al. 2007). Optical and NIR (JHK) interferometry reveals complex and time-varying structures on subarcsecond scales close to the star (Tuthill et al. 2000, 2005; Weigelt et al. 2002). Non-spherical structures were also revealed in linear polarization maps produced by dust scattering at $0.''25$ resolution in H band (Murakawa et al. 2005).

A previous polarization detection in IRC+10216 was reported by (Glenn et al. 1997) for the CS 2–1 line. In this letter, we present the detection of the linear polarized emission for the CO 3–2 SiS 19–18 and CS 7–6 lines in IRC+10216. This is the first time that maps of the linear polarized emission in IRC+10216

are presented.

2. Observations

The SMA observations were taken on 2010 November 24 in the compact configuration. The receiver was tuned to cover the 330.6-334.5 and 342.6-346.5 GHz frequencies in the lower (LSB) and upper side band, (USB) respectively. The phase center of the telescope was RA(J2000.0)= $9^{\rm h}47^{\rm m}57\overset{\rm s}{.}38$ and DEC(J2000.0)= $13^\circ16'43\overset{''}{.}70$. The correlator provided a spectral resolution of about 0.8 MHz (i.e., 0.7 km s^{-1} at 345 GHz). The gain calibrators were QSOs J0854+201 and J1058+015 . The bandpass and polarization calibrator was 3c454.3, which was observed in a parallactic angle range of $\sim 120^\circ$. The absolute flux scale was determined from observations of Titan. The flux uncertainty was estimated to be $\sim 20\%$. The data were reduced using the MIRIAD software package (Wright & Sault 1993). The SMA conducts polarimetric observations by cross correlating orthogonal circularly polarizations (CP). The CP is produced by inserting quarter wave plates in front of the receivers which are inherently linearly polarized. A detailed description of the instrumentation techniques as well as calibration issues is discussed in Marrone & Rao (2008) and Marrone et al. (2006). In order to obtain a more accurate polarization calibration, we solve for the leakage solution independently for the strongest detected lines (CO and ^{13}CO 3–2, H^{13}CN 3–2, CS 7–6 and SiS 19–18) by selecting a frequency range of $\simeq$ 1.5 GHz centered within 0.1 GHz with respect to the rest frequency of each line. We found polarization leakages between 1 and 2% for the USB, while the LSB leakages were between 2 and 4%. These leakages were measured to an accuracy of 0.1%. Self-calibration was performed independently for the USB and LSB on the continuum emission of IRC+10216. All maps were done with Natural weighting in order to maximize the sensitivity, which yielded a synthesized beam of $2\overset{''}{.}6 \times 1\overset{''}{.}6$ with a position angle of PA$\simeq 0^\circ$ (see caption of Figure 2 for more specific values). Significant polarization was only detected in the CO 3–2, CS 7–6 and SiS 7–6 lines, so this paper presents and discuss the detection significance for these three lines.

3. Results and analysis

Figure 1 shows the Stokes I, Q and U obtained at the positions of maximum polarized intensity for the CO 3–2, CS 7–6 and SiS 19–18 lines. Figure 2 shows the polarization maps for the emission of these lines averaged over the velocity range that maximizes the polarized emission, which is different for each line.

The CO 3-2 lines is the strongest line detected in our observations (the line is 50% brighter than the other two lines in the shortest baselines of the visibility plane). This line emission is known to be spatially very extended, much beyond the primary beam of the SMA antennas (Truong-Bach et al. 1991). However the SMA filters out the CO emission that arises from structures larger than about $10''$ (Girart et al. 2006), so the detected emission appears relatively compact. Indeed, the CO averaged emission over the blueshifted component shown in Fig. 2 has a relatively compact component (with a radius of $\simeq 2''$), surrounded by a weak components that extends up $5''$ from the center at an intensity level of about 5% of the maximum. The CS and SiS show also a compact component with similar dimensions, but they lack the weaker and extended component. The Stokes I emission of the 3 lines has a similar brightness, $\simeq$ 120 K for the CS and SiS and 150 K for CO.

The rms noise of the Stokes Q and U emission appears to slightly increase in the channels where the line emission is brightest. This effect is seen in the three lines, though at different levels, from a maximum increase of 5%, 13% and 20% for the CS, SiS and CO lines, respectively. This increase is probably produced

by the residual leakage (estimated to be of $\simeq 0.1\%$, Marrone & Rao 2008) as the total intensity is very strong in the central channels. The larger increase for the CO may be due because it is the most extended and the brightest line (specially the shortest baselines). Taking into account this increase of noise, there is still significant emission in the Stokes Q and U maps of the SiS at the $\simeq 6$-σ level, and in CO and CS lines at the $\simeq 5$-σ level. The linear polarization maps were computed by using a 3-σ cutoff, where σ is the rms noise in the map where the polarization is detected.

The CO linear polarization arises from both the U and Q components, being relatively bright in the later. The CS and SiS lines show mainly polarized emission in the U component. Interestingly, the polarized emission in the three lines appears to be blueshifted with respect to the total intensity.

In order to derive the polarization pattern in the plane of the sky, we have computed polarization maps with the emission averaged over the velocity range where the polarization intensity is detected (see Figure 2). The polarization degree at the position where it is strongest is of $\simeq 2\%$ for the CO and SiS lines, and of $\simeq 4\%$ for the CS. The CO 3–2 polarization arises from two spots, one at the center of IRC+10216 and the other located $\simeq 3''$ to the East. The polarization vectors are oriented roughly North-South, changing slightly from a position angle of $PA = -11^\circ$ at the eastern spot, to -25° at the central spot. The SiS 19–18 polarized emission arises mainly from the north-eastern quadrant of the IRC+10216 envelope (the polarization peak is located $\simeq 2\farcs6$ from the center's envelope). There are two other small spots, with a polarized emission too marginal to be further considered here. The polarization of the main component has a mean position angle of about -41°, but the pattern of the polarization vectors appear to form an arc, following roughly the contours of the Stokes I emission. The CS 7–6 polarization arises from the envelope's south-western quadrant (the polarization peak is located $\simeq 2\farcs9$ from the center's envelope). The polarization PA pattern is quite uniform with an averaged value of $\simeq 48^\circ$.

The SiS polarization vectors' pattern suggest a radial distribution. Therefore, we have compared the polarization vector direction with the expected radial direction (with respect to the envelope center) at the position the vectors. Figure 3 shows the difference between the polarization vectors and the radial directions. On one hand, the SiS polarization vectors are all almost perpendicular to the radial direction, i.e., they form a nearly perfect concentric arc-like pattern with respect to the envelope's center. On the other hand and despite the low polarization statistics, this is not the case for the CO and CS polarization vectors.

4. Discussion and conclusions

The detailed analysis of population of the magnetic sub-levels in rotational lines show that the highest polarized emission is expected for volume densities similar to the critical density of the observed transition, and depending on the transition and on the molecule, the polarization can still be significant even at densities ten times higher (Deguchi & Watson 1984). This suggests that the polarization detected in the CO 3–2 line should arise at volume densities of $\sim 10^4$ cm^{-3}, so at the outer regions of the shell, whereas the the SiS 19–18 and CS 7–6 polarization is expected to trace inner regions, at densities of $\sim 10^7$ cm^{-3}.

One of the interesting features is that in the three lines the linear polarization is blueshifted with respect to the total emission (this effect is more significant in the SiS line). Considering that the envelope is expanding, this suggest that the polarized emission is being detected at the side of a shell facing us and with the aforementioned volume densities. In addition, most of the polarized emission arises about $3''$ offset ($\simeq 450$ AU in projection) of the envelope's center. Thus the optical depth is probably playing an important role. Indeed, subarcsecond resolution maps in the IR (Menut et al. 2007; Leão et al. 2006) and HCN 3–2

emission (Shinnaga et al. 2009) show that the molecular distribution is asymmetrical. This suggests the anisotropy in the radiation field to be a cause for the polarization pattern to be not distributed spherically. This is also in agreement with the single-dish detection of the CS 2–1 line polarization towards the center of IRC+10216, which suggests that there is a non-radial polarization pattern (Glenn et al. 1997).

In circumstellar envelopes and for mm molecular lines the Zeeman splitting is much larger than the collision and spontaneous rates, even for magnetic fields strength of only few μG. Therefore, the polarization should be aligned parallel or perpendicular to the magnetic field (Kylafis 1983; Morris et al. 1985). An overall radial magnetic field is expected if it is weak enough to be energetically irrelevant, i.e., the magnetic energy is significantly smaller than the mechanical energy of the stellar wind: $B \ll (\dot{m} v_t)^{1/2} (D\Omega)^{-1}$, where $\dot{m}$ is the mass loss rate, v_t the terminal velocity, D the distance of IRC+10216 and Ω the angular radius (Glenn et al. 1997). Using the measured values in IRC+10216 (see § 1) and at the distance where the polarization is detected ($\simeq 3''$, 450 AU), this condition is satisfied if $B \ll 8$ mG. CN Zeeman splitting observations in IRC+10216 indicate a strength of $\simeq 9$ mG at a larger distance (2500 AU, Herpin et al. 2009) . For a solar-type and toroidal magnetic field configuration ($B \propto r^{-2}$ and r^{-1}, respectively; Vlemmings 2011) the expected strength where the polarization is detected would be in the 50 to 300 mG range. Therefore, the magnetic field is strong enough to not be radially shaped by the wind.

The measured polarized vectors can be either parallel or perpendicular to the projected magnetic field direction in plane-of-the-sky (Kylafis 1983). A proper radiative transfer analysis and a model of the physical conditions of the envelope (including the magnetic field configuration) is needed to solve for this degeneracy. This applies for the measured CO and CS polarization maps. Nevertheless, in the region where the SiS polarization is detected, the polarization pattern is indicative of a radial magnetic field (see Fig. 3). Theoretical studies show that in an expanding circumstellar envelope with a radial magnetic field, the polarization will be parallel (or perpendicular) to the radial direction if it arises at radii lower (or higher) than at certain impact parameter, R_J (Deguchi & Watson 1984; Morris et al. 1985). R_J is the radius where the spontaneous emission rate for the $J \rightarrow J-1$ transition is equal to the IR absorption rate. According to Morris et al. (1985), in IRC+10216 the value of R_J for the SiS 2–1 line is $R_2 \simeq 5 \times 10^{16}$ cm. The spontaneous emission rate increases with J as $J^4/(2J+1)$, and the IR absorption rate goes as R^{-2}, so $R_{19} \simeq 2 \times 10^{15}$ cm. The region where SiS 19–18 polarization is detected arises at a radius of $\simeq 5 \times 10^{15}$ cm from the star. Therefore the SiS 19–18 polarization pattern is in agreement with the theoretical predictions if the magnetic field is radial in the region where SiS the polarization is detected.

In summary, we have detected and mapped the polarization pattern for the first time in IRC+10216, through spectro-polarimetric observations of the CO 3–2, SiS 19–18 and CS 7–6 lines. Although, the data obtained so far lack the sensitivity to allow us to make specific predictions on the magnetic configuration of the IRC+10216 envelope, the polarization pattern measured discards that the magnetic field configuration has a global radial pattern (this is only observed locally where the SiS 19–18 polarization is detected), but it possibly has a rather complex magnetic field morphology. In addition, the polarization detection in three different molecular lines implies that with the higher sensitivity and angular resolution that the Atacama Large Millimeter Array is going to provide, it would be possible to carry out spectro-polarimetric observations for a tomographic imaging of the magnetic field in circumstellar envelopes. However, the ambiguity between the polarization direction with respect to the magnetic field direction, implies that in order to properly relate the polarization pattern with the magnetic field, a complete radiative transfer analysis should be made.

We thank all members of the SMA staff that made these observations possible. JMG is supported by the Spanish MICINN AYA2008-06189-C03 and the Catalan AGAUR 2009SGR1172 grants. WV acknowledges

support by the Deutsche Forschungsgemeinschaft (DFG) through the Emmy Noether Research grant VL 61/3-1.

REFERENCES

Amiri, N., Vlemmings, W., & van Langevelde, H. J. 2011, A&A, 532, A149

Cortes, P. C., Crutcher, R. M., & Watson, W. D. 2005, ApJ, 628, 780

Crosas, M., & Menten, K. M. 1997, ApJ, 483, 913

Deguchi, S., & Watson, W. D. 1984, ApJ, 285, 126

Etoka, S., & Diamond, P. 2004, MNRAS, 348, 34

Fonfría Expósito, J. P., Agúndez, M., Tercero, B., Pardo, J. R., & Cernicharo, J. 2006, ApJ, 646, L127

Forbrich, J., Wiesemeyer, H., Thum, C., Belloche, A., & Menten, K. M. 2008, A&A, 492, 757

Girart, J. M., Beltrán, M. T., Zhang, Q., Rao, R., & Estalella, R. 2009, Science, 324, 1408

Girart, J. M., Crutcher, R. M., & Rao, R. 1999, ApJ, 525, L109

Girart, J. M., Rao, R., & Marrone, D. P. 2006, Science, 313, 812

Glenn, J., Walker, C.K., Bieging, J.H., & Jewell, P. R. 1997, ApJ, 487, 89

Goldreich, P., Kylafis, N. D. 1981, ApJ, 243, L75

Goldreich, P., Kylafis, N. D. 1982, ApJ, 253, 606

Herpin, F., Baudry, A., Thum, C., Morris, D., & Wiesemeyer, H. 2006, A&A, 450, 667

Herpin, F., Baudy, A., Josselin, E., Thum, C., & Wiesemeyer, H. 2009, IAU Symposium, 259, 47

Kemball, A. J., Diamond, P. J., Gonidakis, I., et al. 2009, ApJ, 698, 1721

Kylafis, N. D. 1983, ApJ, 267, 137

Lai, S.-P., Girart, J. M., & Crutcher, R. M. 2003, ApJ, 598, 392

Leão, I. C., de Laverny, P., Mékarnia, D., de Medeiros, J. R., & Vandame, B. 2006, A&A, 455, 187

Marrone, D. P., Moran, J. M., Zhao, J.-H., & Rao, R. 2006, ApJ, 640, 308

Marrone, D. P., & Rao, R. 2008, Proc. SPIE, 7020

Mauron, N., & Huggins, P. J. 1999, A&A, 349, 203

Men'shchikov, A. B., Balega, Y., Blöcker, T., Osterbart, R., & Weigelt, G. 2001, A&A, 368, 497

Menut, J.-L., Gendron, E., Schartmann, M., et al. 2007, MNRAS, 376, L6

Morris, M., Lucas, R., & Omont, A. 1985, A&A, 142, 107

Murakawa, K., Suto, H., Oya, S., et al. 2005, A&A, 436, 601

Patel, N. A., Young, K. H., Gottlieb, C. A., et al. 2011, ApJS, 193, 17

Rao, R., Girart, J. M., Marrone, D. P., Lai, S.-P., & Schnee, S. 2009, ApJ, 707, 921

Shinnaga, H., Young, K. H., Tilanus, R. P. J., et al. 2009, ApJ, 698, 1924

Tenenbaum, E. D., Dodd, J. L., Milam, S. N., Woolf, N. J., & Ziurys, L. M. 2010, ApJ, 720, L102

Truong-Bach, Morris, D., & Nguyen-Q-Rieu 1991, A&A, 249, 435

Tuthill, P. G., Monnier, J. D., Danchi, W. C., & Lopez, B. 2000, ApJ, 543, 284

Tuthill, P. G., Monnier, J. D., & Danchi, W. C. 2005, ApJ, 624, 352

Vlemmings, W. H. T. 2011, Asymmetric Planetary Nebulae V, p. 89

Vlemmings, W. H. T., Humphreys, E. M. L., & Franco-Hernández, R. 2011, ApJ, 728, 149

Vlemmings, W. H. T., Ramstedt, S., Rao, R., & Maercker, M. 2012, A&A, 540, L3

Vlemmings, W. H. T., van Langevelde, H. J., & Diamond, P. J. 2005, A&A, 434, 1029

Weigelt, G., Balega, Y. Y., Blöcker, T., et al. 2002, A&A, 392, 131

Wright, M. C. H., & Sault, R. J. 1993, ApJ, 402, 546

Young, et al. 1993

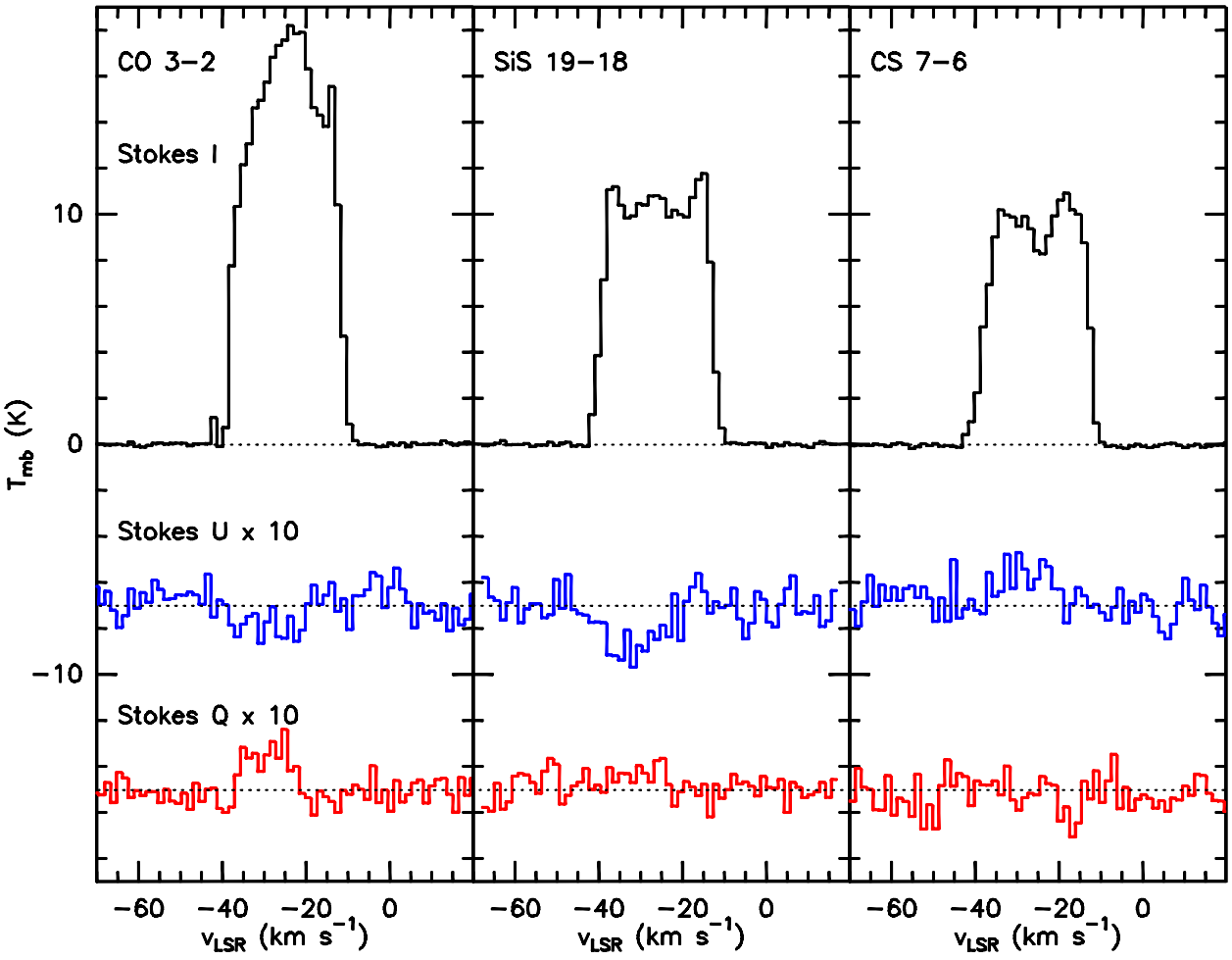

Fig. 1.— Spectra of the Stokes I (top, black line), U (center, blue line) and Q (bottom, red line) emission of the CO J=3–2 (left panel), SiS J=19–18 (central panel) and CS J=7–6 lines (right panel). For each line this spectrum was taken at the position where the maximum polarized emission is detected, after convolving the maps with a Gaussian having a FWHM of $4'' \times 3''$.

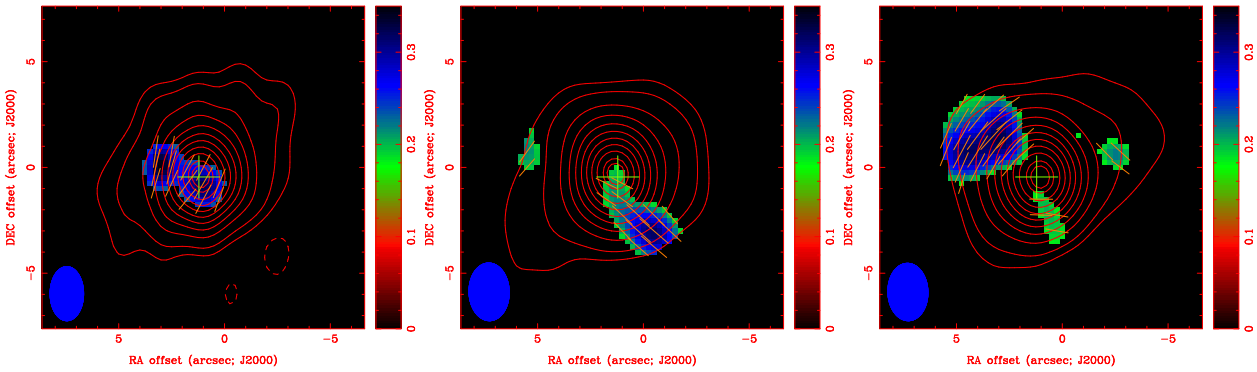

Fig. 2.— Color image of the linearly polarized intensity of the CO 3–2 (left panel), SiS 19–18 (central panel) and CS 7–6 lines (right panel), overlapped with the contour maps of the I emission for the respective lines. The orange bars represent the polarization vectors. The CS and CO maps show the emission at the $v_{\rm LSR}$ velocity of -29 km s^{-1} averaged over 16 km s^{-1}. The SiS map shows the emission at $v_{\rm LSR}$ =-31.5 km s^{-1} averaged over 20 km s^{-1}. The contour levels are 5, 10, 20, 30, 40, 50, 60, 70, 80, 90, 95% of the peak intensity. The wedge shows the polarized intensity scale in units of Jy beam^{-1} . The synthesized beam is shown in the bottom left corner of each panel.

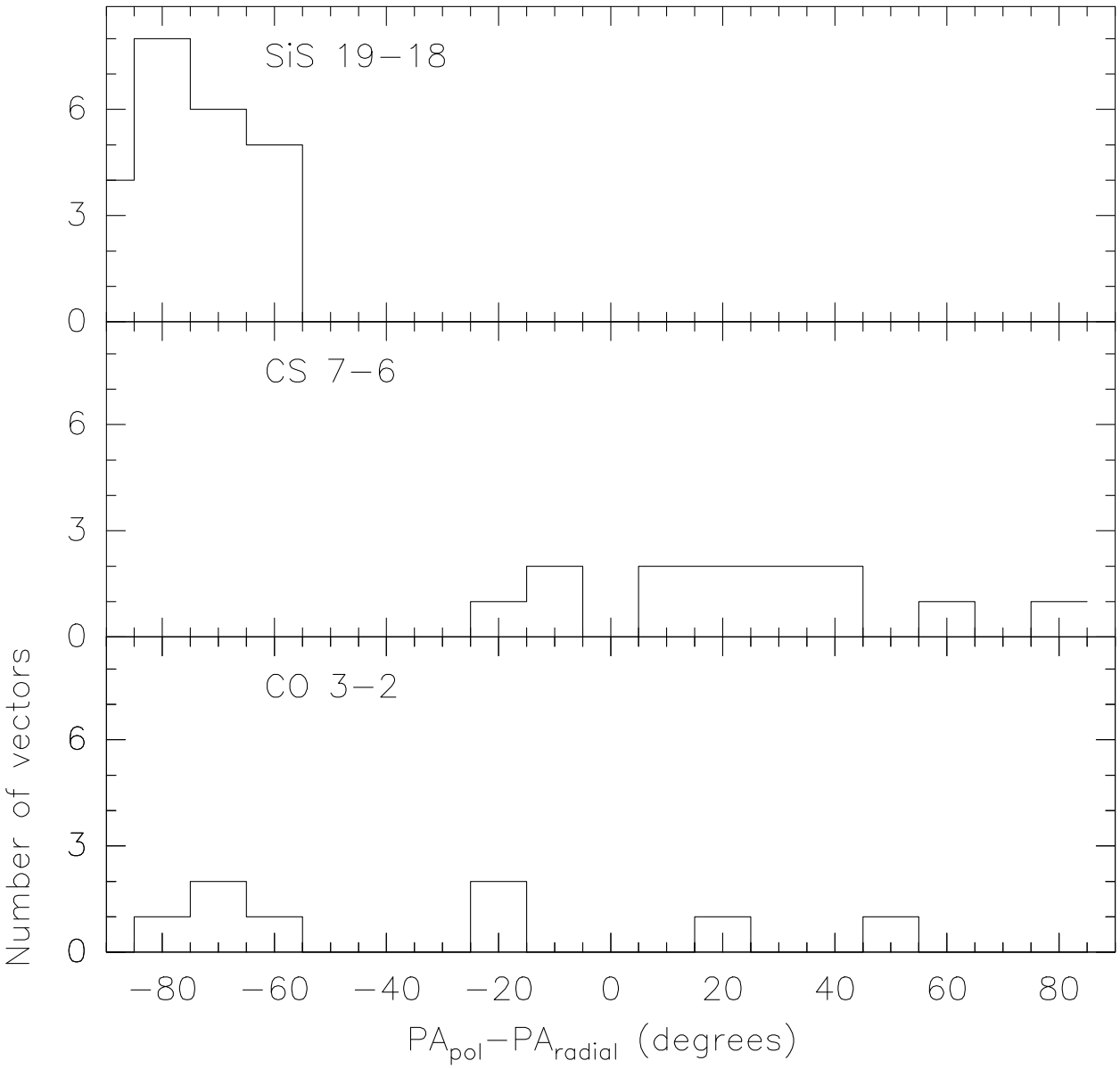

Fig. 3.— Distribution of the difference between the position angle of the SiS, CS and CO polarization vectors and the radial direction with respect to the center of the envelope. We have used a Nyquist sample of the polarization vectors to compute this difference, excluding the vector closer than $\simeq 1''$ from the envelope center.